

# A 3D-Structured Sustainable Solar-Driven Steam Generator Using Super-Black Nylon Flocking Materials

Ce Tu, Wenfu Cai, Xue Chen,\* Xiaolong Ouyang, Hui Zhang,\* and Zhong Zhang\*

Solar-driven evaporation is a promising way of using abundant solar energy for desalinating polluted water or seawater, which addresses the challenge of global fresh water scarcity. Cost-effectiveness and durability are key factors for practical solar-driven evaporation technology. The present cutting-edge techniques mostly rely on costly and complex fabricated nanomaterials, such as metallic nanoparticles, nanotubes, nanoporous hydrogels, graphene, and graphene derivatives. Herein, a black nylon fiber (BNF) flocking board with a vertically aligned array prepared via a convenient electrostatic flocking technique is reported, presenting an extremely high solar absorbance (99.6%), a water self-supply capability, and a unique salt self-dissolution capability for seawater desalination. Through a carefully designed 3D structure, a plug-in-type BNF flocking board steam generator realizes a high evaporation rate of  $2.09 \text{ kg m}^{-2} \text{ h}^{-1}$  under  $1 \text{ kW m}^{-2}$  solar illumination, well beyond its corresponding upper limit of  $1.50 \text{ kg m}^{-2} \text{ h}^{-1}$  (assuming 100% solar energy is being used for evaporation latent heat). With the advantages of high-efficiency fabrication, cost-effectiveness, high evaporation rate, and high endurance in seawater desalination, this 3D design provides a new strategy to build up an economic, sustainable, and rapid solar-driven steam generation system.

fresh water scarcity for at least 5 months of a year, and about 4 billion people have a severe fresh water scarcity problem for at least 1 month of a year. Moreover, it was predicted that by 2025, over 50% of the nations in the world will face fresh water scarcity, and by 2050, about 75% of the world's populations could face water scarcity.<sup>[4–6]</sup> Solar energy, as the most abundant, pollution-free, and inexhaustible natural energy source, has been widely utilized in the solar-driven water evaporation technique, which shows the great potential for water purification and seawater desalination.<sup>[7–10]</sup>

Unlike the conventional solar-driven steam generators, which involve heating the bulk water and suffer from inferior energy conversion efficiency,<sup>[11,12]</sup> the novel solar-driven steam generator by the surface localized-heating behavior commonly has a high solar absorbing surface and can float on the water surface.<sup>[13–21]</sup> So far, a variety of newly emerging nanomaterials have been widely explored in solar-driven evaporation applications due to their

## 1. Introduction


Fresh water scarcity is a global crisis that continues to worsen due to environmental pollution, population increase, and climate change.<sup>[1–3]</sup> Many areas around the world suffer from

effective solar absorbance and high solar steam generation efficiency, such as gold nanoparticles, aluminum nanoparticles, carbon nanotube, graphene and their derivatives, etc.<sup>[13–19]</sup> Under 1 sun illumination ( $1 \text{ kW m}^{-2}$ ), a high evaporation rate of  $1.63 \text{ kg m}^{-2} \text{ h}^{-1}$  has been reached by an evaporator consists of cotton-CuS nanocage-agarose aerogel.<sup>[15]</sup> However, as is well known, there are still tremendous challenges of nanomaterials that need to be addressed including material cost, severe preparation process as well as scale-up production. Therefore, research efforts related to the development of solar-driven steam generators composed of cheap and large scalable materials have recently flourished: Gan's group reported an efficient carbon-based solar vapor generation system based on extremely low-cost carbon-coated paper (CP) affixed to expanded polystyrene foam, which realized a high energy conversion efficiency of 88% for steam generation under  $1 \text{ kW m}^{-2}$  solar illumination, corresponding to an evaporation rate of  $1.28 \text{ kg m}^{-2} \text{ h}^{-1}$ .<sup>[20]</sup> Ji's group designed and developed a new polymer foam by synthesizing oligoaniline for solar-driven water evaporator. The polymer foam is easy to prepare and scale up from low-cost raw chemicals. Under  $1 \text{ kW m}^{-2}$  solar illumination, its evaporation rate could reach  $1.16 \text{ kg m}^{-2} \text{ h}^{-1}$  with excellent durability and stability.<sup>[21]</sup> To be fair, it should be pointed out that both the CP and the polymer foam involved chemical solvents and

Dr. C. Tu, W. F. Cai, Prof. H. Zhang, Prof. Z. Zhang  
CAS Key Laboratory of Nanosystem and Hierarchical Fabrication  
CAS Center for Excellence in Nanoscience  
National Center for Nanoscience and Technology  
Beijing 100190, China  
E-mail: zhangh@nanoctr.cn; zhong.zhang@nanoctr.cn

Prof. X. Chen  
School of Mechanical and Electrical  
Beijing University of Chemical Technology  
Beijing 100029, China  
E-mail: xchen@buct.edu.cn

Dr. X. L. Ouyang  
Department of Energy and Mineral Engineering and EMS Energy  
Institute  
The Pennsylvania State University  
University Park, PA 16802, USA

 The ORCID identification number(s) for the author(s) of this article can be found under <https://doi.org/10.1002/sml.201902070>.

DOI: 10.1002/sml.201902070

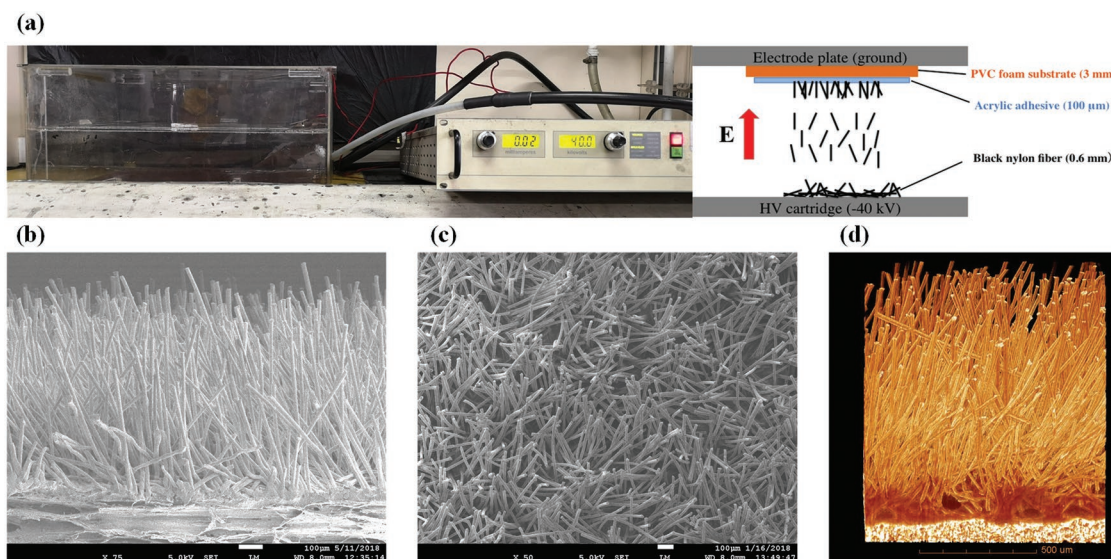


**Figure 1.** a) Photo image and schematic of the electrostatic flocking device. SEM images of the BNF flocking board in b) the side view and c) the top view. d) The morphology of the BNF flocking board characterized by Micro CT.

multistep preparation method in the fabrication process, which are still the significant bottlenecks for practical applications. Considering the feasibility and scalability, finding a more cost-effective and scalable strategy to fabricate efficient solar-driven steam generator is highly expected, especially in energy deficient and industrially underdeveloped regions.

Herewith, we introduce a convenient electrostatic flocking technique to prepare the highly efficient solar-driven steam generators,<sup>[22,23]</sup> with vertically aligned, high-density array of black nylon fibers (BNFs) on a planar polyvinyl chloride (PVC) foam substrate, which is named as BNF flocking board. Owing to the vertical and dense BNF array, the BNF flocking board possesses an extremely high solar absorbance (99.6%) and a unique wicking ability simultaneously. PVC foam substrate shows a low density and a high thermal resistance, thus the BNF flocking board has successive combinations of high solar absorbance, flotation ability, thermal insulation, and water self-supply parts. Under  $1 \text{ kW m}^{-2}$  solar illumination, its evaporation rate is  $1.10 \text{ kg m}^{-2} \text{ h}^{-1}$ . Additionally, the BNF flocking board exhibits a good durability and stability under real seawater evaporation condition, furthermore, the accumulated salt on the board surface can partially dissolve and transport back to the surrounding seawater in dark environment due to its diffusion ability. More importantly, we fully took advantage of designability of the BNF flocking board, designed a plug-in structural steam generator by composing multi-surface BNF flocking boards, which realized an intriguing evaporation rate of  $2.09 \text{ kg m}^{-2} \text{ h}^{-1}$  under  $1 \text{ kW m}^{-2}$  solar illumination, well beyond the theoretical limit of  $1.50 \text{ kg m}^{-2} \text{ h}^{-1}$  (assuming 100% solar energy was being used for evaporation latent heat).<sup>[20]</sup> Because of this, electrostatic flocking fabrication approach is cost-effective, scalable, and widely used in industry, designable BNF flocking board steam generator shows high potentials to build up a scalable solar-driven evaporation system for mass production of clean water.

## 2. Results and Discussion

### 2.1. Vertically Aligned Array of the BNF Flocking Board, and its Solar Absorbance and Wicking Ability

The BNF flocking board was prepared via a one-step electrostatic flocking technique (Figure 1a). As shown in Figure 1b,c, we observed that the electrostatic flocking is a very effective approach to fabricate a high-density and uniform array of vertically aligned BNF. The flocking density of the BNF was  $116.1 \text{ g m}^{-2}$  as measured by gravimetric analysis, the flocking density affects the various properties of BNF flocking board (Figure S1a, Supporting Information), the BNF flocking board with flocking density of  $116.1 \text{ g m}^{-2}$  was an optimized selection. Additionally, the microstructure of vertically aligned array also can be observed by the Micro CT (Figure 1d), the depth of nylon fibers in the acrylic adhesive was about  $50 \mu\text{m}$ , and the volume ratio of nylon fibers was about 17 vol%, as calculated by 3D Viewer analysis.

Although the vertically aligned array of BNF flocking board was not completely optimized, that structure still endows the board an extremely high solar absorbance and a unique wicking ability simultaneously. The comparison of solar absorbance between the PVC foam substrate and the BNF flocking board is shown in Figure 2a. Compared with the PVC foam substrate, the BNF flocking board shows an ultra-high absorbance with an average of about 99.6% throughout the visible to near IR domain from 280 to 2500 nm (Figure S1b, Supporting Information), which reveals that vertically aligned array of BNF plays an important role in enhancing the solar absorbance. This strong broadband solar absorbance is particularly promising for effective solar-thermal conversion.<sup>[24,25]</sup> The BNF flocking board also exhibits a good thermal stability (Figure S1c, Supporting Information). Under  $1 \text{ kW m}^{-2}$  solar illumination, the temperature of the BNF flocking board surface rapidly increased from 25.0 to 73.5 °C in 3 min. In contrast, the  $\Delta T$  of PVC foam substrate only increased from 27.0 to 36.4 °C (Figure 2b), representing

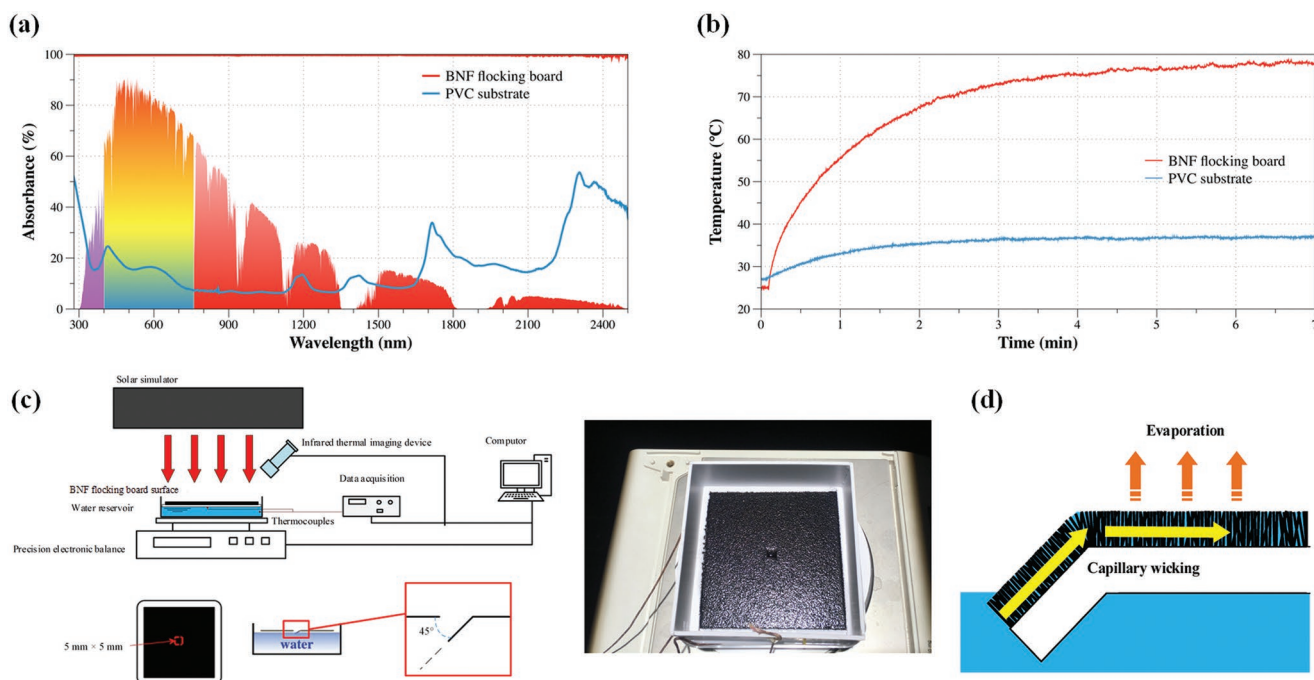


**Figure 2.** a) The solar absorbance spectra of PVC foam substrate (blue) and BNF flocking board (red) measured by a spectrophotometer equipped with an integration sphere. The background of colored region represents the solar spectrum. b) The temperatures changing of PVC foam substrate (blue) and BNF flocking board (red) as a function of time under  $1 \text{ kW m}^{-2}$  solar illumination. c) Schematic illustration and photo image of the setup of the water evaporation measurement with the BNF flocking board floating on the water surface during evaporation process. d) Schematic mode of the BNF flocking board floating on the water surface during evaporation process.

the outstanding solar-thermal conversion property of the vertically aligned array of BNF flocking board. Beside an ideal solar absorbing performance, the vertically aligned array of BNF flocking board possesses a unique water self-supply ability simultaneously, which makes the liquid transport rapidly due to the wicking effect.<sup>[26,27]</sup> The surface wettability has been considered as one of the important factors for water transportation during evaporation.<sup>[28–30]</sup> The images (Figure S2, Supporting Information) captured by a high-speed camera showed that the water droplet spreads and wicks quickly after it touches the BNF flocking board surface. Due to the wicking ability, the high-speed camera hardly obtains the water contact angle of the BNF flocking board. Hence, the water contact angle of BNF flocking board can be considered as  $0^\circ$ . A series of experiments were performed with the schematic shown in Figure 2c and details are in the Experimental Section to analyze wicking ability of the BNF flocking board. Figure 2d shows a schematic mode of the BNF flocking board floating on the water surface during evaporation process, this model estimated the maximum radius  $R^*$  of the present BNF flocking board under saturated evaporation condition (under  $1 \text{ kW m}^{-2}$  solar illumination) and maximum heat flux  $q_{\text{max}}$  for present BNF flocking board with solar radiation further. The estimation is considered based on following assumptions: a) the surface was wetted completely; b) the whole capillary force was used to overcome the flow resistant. Consequently, the maximum radius  $R^*$  of the present BNF flocking board under saturated evaporation condition (under  $1 \text{ kW m}^{-2}$  solar illumination) is 13.2 cm, and the maximum heat flux for the present BNF flocking board can withstand is  $9.5 \text{ kW m}^{-2}$ , these results indicate that the BNF flocking

board has high potentials for applications under various conditions, concentrated solar illumination, or insufficient water supplement (for detailed derivation process, see Section S3, Supporting Information).

## 2.2. The BNF Flocking Board for Solar-Driven Steam Generation

The same BNF flocking board tested in the characterization of wicking ability was also used in the solar-driven evaporation. As shown in Figure 3a, under  $1 \text{ kW m}^{-2}$  solar illumination, the weight loss rate of the BNF flocking board is  $6.37 \text{ g h}^{-1}$  and the evaporation rate could reach  $1 \times 10 \text{ kg m}^{-2} \text{ h}^{-1}$  (after 40 min illumination), which is about 2.62 times higher than that of pure water under the same  $1 \text{ kW m}^{-2}$  solar illumination. The steam generation efficiency ( $\eta$ ) was calculated based on the following Equation (1)

$$\eta = \frac{\dot{m}(H_{\text{LV}} + Q)}{E_{\text{in}}} \quad (1)$$

where  $\dot{m}$  refers to the evaporation rate ( $\text{kg m}^{-2} \text{ h}^{-1}$ ) (with the dark evaporation over the BNF flocking board of  $0.02 \text{ kg m}^{-2} \text{ h}^{-1}$  subtracted),  $H_{\text{LV}}$  refers to the total enthalpy that is required to cause the transition of water from its liquid to vapor phase  $H_{\text{LV}}(T_e) = 1.91846 \times 10^6 \times [T_e/(T_e - 33.91)]^2 \text{ J kg}^{-1}$ ,  $T_e$  is the temperature of evaporation (316.6 K),  $Q$  is the sensible heat of water of unit mass ( $Q = c \times (T_e - T_0) \text{ J kg}^{-1}$ ), where  $c$  is the specific heat of water which is  $4.2 \times 10^3 \text{ J kg}^{-1} \text{ K}^{-1}$ ,  $T_0$  is the temperature of water (311.8 K) and  $E_{\text{in}}$  ( $\text{kJ m}^{-2} \text{ h}^{-1}$ ) refers to

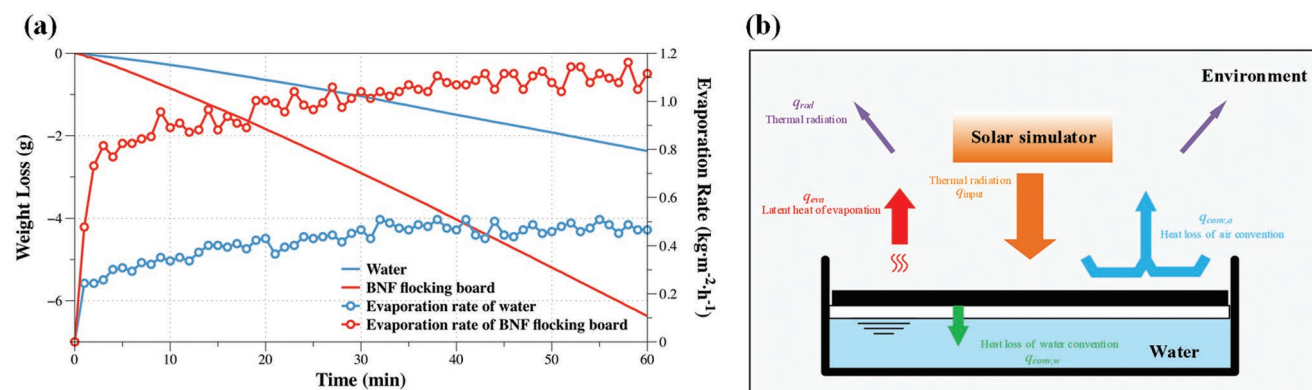


**Figure 3.** a) Comparison of water weight change (line) and evaporation rate (circle) versus time under two different conditions: water (blue) and floating BNF flocking board (red) under  $1 \text{ kW m}^{-2}$  solar illumination. b) Energy dissipation of the BNF flocking board floating on the water surface under  $1 \text{ kW m}^{-2}$  solar illumination.

the total solar energy input per unit time on the system.<sup>[31]</sup> The  $\eta$  of the BNF flocking board is around 72.8%, thus the theoretical limit evaporation rate is about  $1.50 \text{ kg m}^{-2} \text{ h}^{-1}$  in our system (assuming 100% solar energy was being used for evaporation latent heat).

Figure 3b shows the energy dissipation to further evaluate the solar-evaporation performance of the BNF flocking board system quantitatively, the thermal equilibrium (Equation (2)) is expressed as follows

$$q_{input} = q_{eva} + q_{rad} + q_{conv,a} + q_{conv,w} \quad (2)$$

where  $q_{input}$  refers to the total input energy as thermal radiation generated by solar simulator,  $q_{eva}$  refers to the evaporative latent heat,  $q_{rad}$  refers to the thermal radiation from the BNF flocking board surface to environment,  $q_{conv,a}$  and  $q_{conv,w}$  are the heat loss by air convection and water convection, respectively.<sup>[32]</sup> Each heat flux is listed in Table 1 and shows the ratio for energy dissipation. Compared with the actual energy input  $q_{input} = 1000 \text{ W m}^{-2}$ , the estimated value of total input energy was  $1025.4 \text{ W m}^{-2}$ , the error with 2.54% is small, which demonstrated the reliability and validity of the present experiment (for more detailed calculations and analysis, see Section S4, Supporting Information).

The thermal equilibrium analysis indicates that the major thermal losses are made by air convection  $q_{conv,a}$  (12.4%) and water convection  $q_{conv,w}$  (11.3%) in the BNF flocking board evaporation systems. The air convection thermal loss  $q_{conv,a}$  could be attributed to the open evaporation experimental condition, the evaporation continuously brought thermal energy from the BNF flocking board surface to ambient air. In the real application, an evaporation collective shield would suppress its air convection thermal loss to a certain extent. On the other

**Table 1.** Heat flux values of energy dissipation for BNF flocking board solar-driven steam system.

	$q_{eva}$	$q_{rad}$	$q_{conv,a}$	$q_{conv,w}$	$q_{input}$
Heat flux ( $\text{W m}^{-2}$ )	732.7	49.5	127.1	116.0	1025.4
Proportion (%)	71.5	4.8	12.4	11.3	100

hand, owing to the surface of BNF flocking board directly contacted with the bulk water, the surface of BNF flocking board with higher temperature lost the heat to bulk water by conduction and water convection, thus the bulk water temperature was continuously increased (Figure S4, Supporting Information), leading to the water convection thermal loss.

### 2.3. Salt Accumulation and Dissolution Behavior of the BNF Flocking Board in Seawater Evaporation Case

For seawater desalination, the solar-driven steam generator is one of the most potential applications. To date, however, the majority of previous solar-driven evaporation technologies were demonstrated using deionized water and thus the salt accumulations issue in seawater desalination was not considered.<sup>[13–18]</sup> There are major unaddressed issues in seawater desalination including salt accumulations, long-term evaporation stability, and durability, which highly influence its application prospects.<sup>[33–36]</sup> As depicted in Figure 4a, in the case of seawater evaporation (seawater sample average salinity  $\approx 2.75 \text{ wt}\%$ , from Bohai Sea, China), the evaporation rates of the BNF flocking board were higher than that of the BNF flocking board floating on the fresh water under  $1 \text{ kW m}^{-2}$  solar illumination at first 2 h, which could be attributed to a lower  $h_{LV}$  of the seawater.<sup>[37]</sup> 2 h later, the evaporation rates of the BNF flocking board in the case of seawater evaporation slightly decreased due to the salt accumulations on the board surface (Figure 4b), the evaporation rates was finally decreased to  $1.02 \text{ kg m}^{-2} \text{ h}^{-1}$  after 8 h seawater evaporation (Figure S5, Supporting Information). These results indicate that in the case of the BNF flocking board under long-term seawater evaporation, the salt crystals accumulate on the board surface and start to reduce the effective evaporation area (Figure 4b and Figure S6, Supporting Information), hence the evaporation has been limited. Moreover, Figure 4b and Figure S6 in the Supporting Information reveal that the salt crystals prefer to accumulate at the edge of the BNF flocking board, which could be mainly attributed to the board in-flow direction of water supply, from the center to the edges. The supplementary water push stray salt ion to the BNF flocking board edges due to the wicking effect, thus the

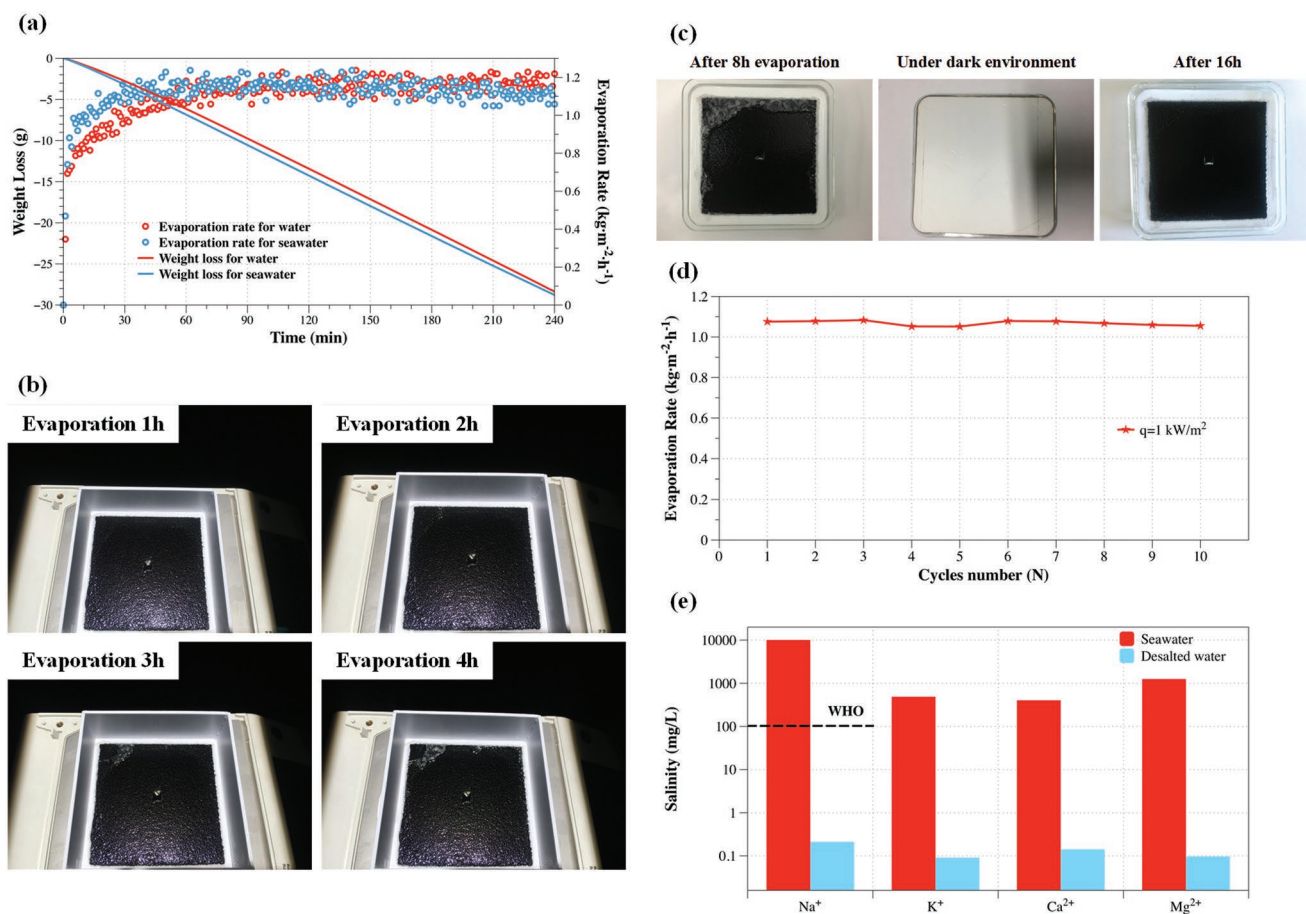


**Figure 4.** a) Comparison of weight change (line) and evaporation rates (circle) of the BNF flocking board floating on water (red) and seawater (blue) versus time under  $1 \text{ kW m}^{-2}$  solar illumination. b) Photo images of the seawater floating BNF flocking board with different evaporation times. c) Photo images of the seawater floating BNF flocking board under different status. d) The evaporation rate of the BNF flocking board samples on salt water as the function of cycle number. e) The measured concentrations of four primary ions in an actual seawater sample (from the Bohai Sea, Bohai Gulf, China; average salinity  $\approx 2.75 \text{ wt}\%$ ) before and after desalination.

board edges became the high salt concentration areas to easily formed salt accumulations.

In some previous works, the salt accumulation issues were commonly overcome by washing the material using water for several times, and in the cyclic solar seawater evaporation, the salt accumulations should be removed by several times water washing after each evaporation.<sup>[19,20]</sup> It should be pointed out that those cyclic solar seawater evaporation experiments are unsuitable for the practical applications in the natural environment. Herein, to test the evaporation stability and sustainability of the BNF flocking board for seawater desalination, we conducted a cyclic solar seawater evaporation experiment. For each cycle, the BNF flocking board had been placed on seawater under  $1 \text{ kW m}^{-2}$  solar illumination for 8 h. After that, the residual seawater in the box was replaced by 95 g new seawater and then the BNF flocking board was placed quietly for 16 h under dark environment for simulating the natural marine environment. After 16 h placement, the BNF flocking board was reused for the next cycle without any washing. In particular, the BNF flocking board shows a unique salt self-dissolution ability, the accumulated salt crystals on the board surface dissolve and transport back to the bulk seawater

automatically at dark condition (Figure 4c). As shown in Figure 4d, the average evaporation rates of ten cycles of seawater floating BNF flocking board are at around  $1.06 \text{ kg m}^{-2} \text{ h}^{-1}$ , indicating a good evaporation stability and salt self-dissolution ability of the BNF flocking board due to the unique porous structure within the BNF flocking board: micro-channel shape and pore size. The vertical aligned array forms rectangular micro-channels, which make the BNF has the larger equivalent mass transfer coefficient and permeability compared with other structures such as foam or interlaced array. Furthermore, the moderate pore size also guarantees the BNF has strong capillary wicking and the space for liquid transport. However, an unideal phenomenon should be noted that some sparingly soluble salt crystals (such as calcium carbonate, calcium sulfate, and magnesium hydroxide) can be clearly observed on the edges of completely dried board after ten cycles of seawater evaporation (Figure S7, Supporting Information). Although the formation of sparingly soluble salt crystals cannot be readily replenished by the water wicking effect, the evaporation rate of the BNF flocking board remains a relative high value ( $1.06 \text{ kg m}^{-2} \text{ h}^{-1}$ ) even after 1 month floating on seawater under natural environment, demonstrating the

sparingly soluble salt accumulations did not noticeably hinder the evaporation performance under ambient solar illumination condition. Considering that the real bulk seawater will provide stronger ion exchange ability toward dissolution of salt accumulations, therefore, the BNF flocking board has a high sustainability for the long-term evaporation in the real seawater environment due to its salt self-dissolution ability. Furthermore, the all four primary ions ( $\text{Na}^+$ ,  $\text{K}^+$ ,  $\text{Ca}^{2+}$ , and  $\text{Mg}^{2+}$ ) concentrations of desalinated seawater were significantly reduced to less than  $1 \text{ mg L}^{-1}$  (Figure 4e), and were below the values obtained through membrane-based ( $10\text{--}500 \text{ mg L}^{-1}$ ) and thermal distillation-based ( $1\text{--}50 \text{ mg L}^{-1}$ ) seawater desalination techniques.<sup>[38]</sup> The quite low ion concentrations ensured that the desalinated seawater was potable.

#### 2.4. 3D-Structured BNF Flocking Board Evaporator Beyond the Theoretical Limit of Evaporation Latent Heat Conversion

Owing to its simultaneously integrated high solar absorbance and water self-supply ability, the BNF flocking board was in favor of a product design, thus we propose a strategy to take advantage of the good designable ability of the BNF flocking board to build a 3D-structured solar-driven steam generator in order to achieve a higher evaporation rate. We fabricated multi-surface BNF flocking board first (Figure S8, Supporting Information), and then vertically inserted multi-surface BNF flocking board into a substrate to develop a plug-in-type BNF flocking board evaporation system (for fabrication details, see Section S6, Supporting Information).

When one multi-surface BNF flocking board was vertically inserted into a PVC foam board, an extremely high evaporation rate of  $19.07 \text{ kg m}^{-2} \text{ h}^{-1}$  under 1 sun illumination was reached (more than six times of any previous records),<sup>[39]</sup> that evaporation rate could be mainly attributed to the vertically inserted multi-surface BNF flocking board. This structure not only increases the evaporation surface area, but also improves the air convection upon BNF surface. (Note: it is the evaporation surface, not the projected area.) An increase in evaporation surface area of  $\approx 43.9 \times (84.32 \text{ cm}^2/1.92 \text{ cm}^2)$  resulted in an  $\approx 17.3 \times (19.07 \text{ kg m}^{-2} \text{ h}^{-1}/1 \times 10 \text{ kg m}^{-2} \text{ h}^{-1})$  increase in total evaporation efficiency. Furthermore, a cold evaporation concept was also used in our plug-in-type BNF flocking board evaporation system,<sup>[40,41]</sup> in which the temperature of the multi-surface board sides ( $26.5 \text{ }^\circ\text{C}$ ) was below the room temperature ( $29.0 \text{ }^\circ\text{C}$ ), gaining energy directly from the environment (sensible heat from air or water) to improve evaporation efficiency (Figure 5a). Although an attractive evaporation rate of  $19.07 \text{ kg m}^{-2} \text{ h}^{-1}$  has been achieved, the projected area of the multi-surface BNF flocking board ( $1.92 \text{ cm}^2$ ) that used to calculate the evaporation rate was unsuitable for the real applications. Herein, we vertically inserted one multi-surface BNF flocking board into a flat BNF flocking board (Figure 5b), the evaporation rate could reach to  $1.27 \text{ kg m}^{-2} \text{ h}^{-1}$ , increased  $\approx 16\%$  compared with that of the flat BNF flocking board evaporator. The best result of evaporation rate is  $2.09 \text{ kg m}^{-2} \text{ h}^{-1}$  when six BNF flocking boards were vertically inserted into a flat BNF flocking board (Figure 5c,d). The obtained evaporation rate of  $2.09 \text{ kg m}^{-2} \text{ h}^{-1}$  is about 1.9 times of the flat BNF flocking board evaporator, and well beyond its corresponding

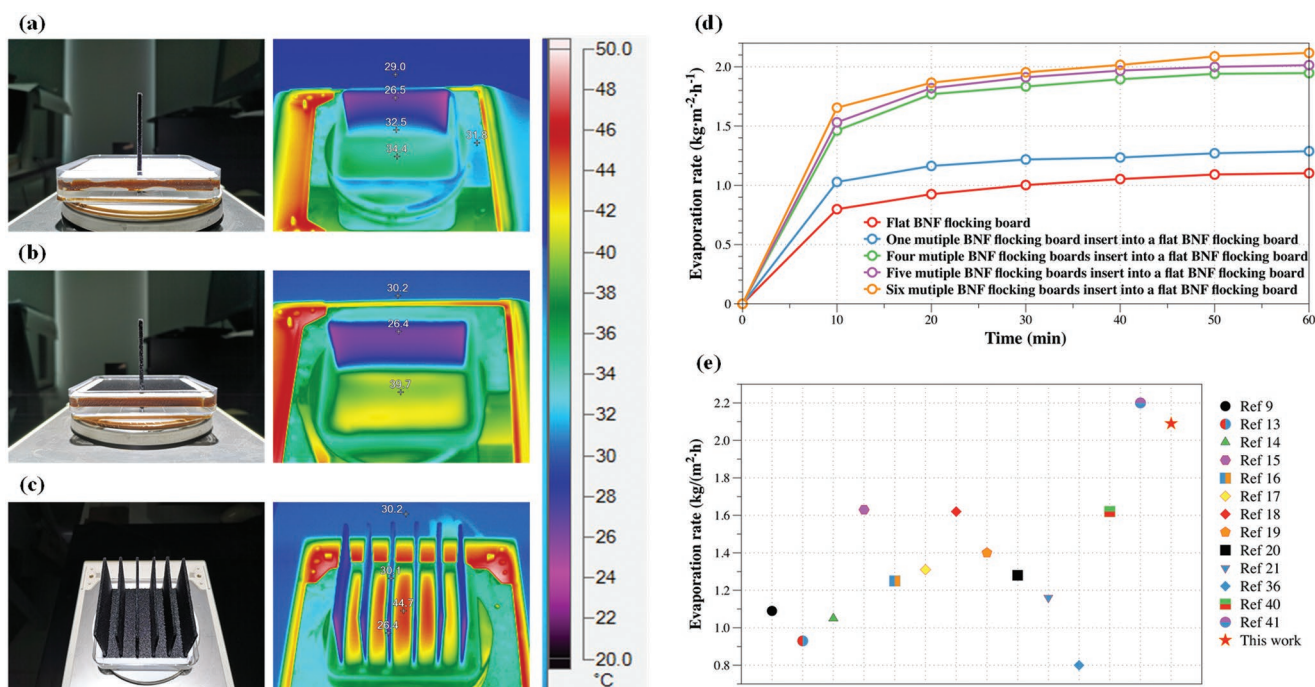


**Figure 5.** Photo and IR images of a) one multi-surface BNF flocking board vertically insert into a PVC board, b) one multi-surface BNF flocking board vertically inserts into a flat BNF flocking board, and c) six multi-surface boards vertically insert into a flat BNF flocking board. d) Evaporation rates of water based on numbers of multi-surface BNF flocking board insert into a flat BNF flocking board versus time under  $1 \text{ kW m}^{-2}$  solar illumination. e) Comparison of the evaporation rate among different evaporators under  $1 \text{ kW m}^{-2}$  solar illumination.

theoretical limit of  $1.50 \text{ kg m}^{-2} \text{ h}^{-1}$  (assuming 100% solar energy was being used for evaporation latent heat), of course better than most previous report records under 1 sun illumination (Figure 5e),<sup>[9,13–21]</sup> even faster than those reported by other systems under 2 sun illumination ( $1.93 \text{ kg m}^{-2} \text{ h}^{-1}$  reported by Ghasemi et al.<sup>[9]</sup>). The significant promotion in evaporation can be explained by the following mechanisms: 1) Reduction in heat loss. The comparison of temperature of flat BNF flocking board surface between Figure 5a and Figure 5c illustrates that the vertical BNF flocking boards can lower the heat loss. This is because the vertical BNF flocking boards block the radiation loss from the BNF flocking board system to surrounding. The narrow gaps between the vertical BNF flocking boards also greatly depress the heat loss by convection. 2) Increment in receiving irradiation. The two side vertical BNF flocking boards increase the exposed area for receiving irradiation from the direct light from the reflected light from surrounding. As a result, the irradiation energy received by the 3D structure of plug-in-type BNF flocking board can be larger than that received by only the bottom area. In a word, the 3D structure of plug-in-type BNF flocking board system is able to break through the 2D limit and has a larger evaporation capacity compared with the flat BNF flocking board.

### 3. Conclusions

In summary, we have reported a solar-driven steam generator based on vertically aligned, high-density array of BNF on a PVC foam substrate prepared by a one-step electrostatic flocking process. The vertically aligned array of BNF endows the board an extremely high solar absorbance (99.6%) and a unique wicking ability, achieving the automatic solar-driven evaporation behavior and a high evaporation rate of  $1.10 \text{ kg m}^{-2} \text{ h}^{-1}$  (solar steam generation efficiency is 72.8%) under  $1 \text{ kW m}^{-2}$  solar illumination. The BNF flocking board evaporator also demonstrates the long-term stability and sustainability in sea-water desalination due to its salt self-dissolution capability. Moreover, an attractive evaporation rate of  $2.09 \text{ kg m}^{-2} \text{ h}^{-1}$  can be achieved under  $1 \text{ kW m}^{-2}$  solar illumination by an advanced 3D structural design.

Except for evaporation and sustainable performances, cost-effectiveness and scalability are essential factors for practical applications. Electrostatic flocking is a one-step, safe, and cost-effective processing method and has been widely used in industrial applications. Utilizing such technology, we can fabricate functional and various structural surfaces on multiple substrates for even about more than 10 000 square meter fabrication. Considering the limit heat flux of solar (upper limit is  $1 \text{ kW m}^{-2}$ ), the solar-driven evaporation system should be particularly promising for personal use in industrially undeveloped regions or energy shortage situations. Our plug-in-type BNF flocking board steam generator has achieved a very high evaporation rate, without any advanced and expensive fabrication method, chemical reagents, and nanomaterials. Thus, the plug-in-type BNF flocking board evaporation system may open up a new way for various fields such as water remediation and desalination.

### 4. Experimental Section

**Materials:** BNFs with a diameter of  $15 \mu\text{m}$  and an average length of  $0.6 \text{ mm}$  were prepared from polyimide 6, the surface of BNF was modified by scouring agents (silica sol and aluminum sol) for electrostatic flocking (Figure S1d, Supporting Information). The acrylic adhesive was an acrylate/polyurethane copolymer emulsion (Figure S1e, Supporting Information). Both of the BNF and acrylic adhesive were provided by Jiahua Printing Co., Ltd., Zhongshan, China. The PVC foam substrate with a thickness of  $3 \text{ mm}$  and the density of  $0.31 \text{ g cm}^{-3}$  was supplied by Yidimei Model Inc., China.

**Preparation of BNF Flocking Board:** On a PVC foam substrate,  $8 \text{ cm} \times 8 \text{ cm}$  square acrylic adhesive was coated in center with a thickness of about  $250 \mu\text{m}$  using a blade coater. A  $100 \mu\text{m}$  thick acrylic adhesive layer was subjected to flocking. As shown in Figure 1a, an electrostatic flocking device with a planar high-voltage cartridge was located under the distributed BNF piles, the adhesive-coated PVC foam substrate was placed on the face of the opposing stainless plate, which plays as an electrode clipped on the ground wire, and a distance of  $10 \text{ cm}$  from the high-voltage cartridge. By applying a potential of  $40 \text{ kV}$  (SL130, P300) between the two plates, the BNF became charged and were propelled toward the opposing electrode because of electrostatic force, thus the BNFs were successfully aligned along the electric field lines between the two electrode plates and inserted into acrylic adhesive layer. Finally, the BNF flocking boards were treated under room temperature for  $24 \text{ h}$  to curing the acrylic adhesive.

**Experiments on Properties of BNF Flocking Board Surface:** A series of experiments were performed aiming to obtain the wicking ability and the solar-driven steam characteristics with the schematic shown in Figure 2c. At first, a box was placed on a high-precision electronic balance with  $45 \text{ g}$  water inside. The prepared BNF flocking board was floated on the water surface, in which, the open area of the box was completely covered by floating the board to eliminate the natural water evaporation effect, and a square of  $5 \text{ mm} \times 5 \text{ mm}$  with three incised boundaries was located in the board center. The incised square with  $45^\circ$  bevel was immersed in the water as a channel for water transport due to the wicking effect (Figure 2c). After the water wetted the whole BNF flocking board surface, the board was illuminated by a solar simulator. The parameters such as the temperature and water mass loss in this overall process were measured. The temperature of BNF flocking board surface was measured by an infrared thermal camera, while the ambient air temperature, board bottom temperature, and bulk water temperature were detected by the thermocouples with error of  $0.4\%$  (Omega, K type) and recorded by a data acquisition (Agilent, 34972A). The mass loss of the water due to evaporation was weighed by a high-precision electronic balance with accuracy of  $1 \text{ mg}$ . The acquisition frequency for all data was  $1 \text{ Hz}$ .

**Characterization:** The microstructures of BNF flocking board were observed using a JSM-7500F scanning electron microscopy (SEM, JEOL Ltd., Japan) at an accelerating voltage of  $5 \text{ kV}$  and a Micro CT (Xradia510 Versa 3D X, ZEISS, German). SEM samples were cut by a blade, then fractured surfaces were sputtered a thin layer of metallic gold on their surface using an Auto Fine Ion Sputter (E-1010, HITACHI Ltd., Japan). The absorbance spectrum was measured by UV-vis-near-infrared spectrophotometer Lambda 950 from  $280$  to  $2500 \text{ nm}$  (Perkin Elmer, USA). An integrating sphere was used to collect the reflected light. The solar illumination using in evaporation experiments was an XES-160S1 3A solar simulator (SAN-EI ELECTRIC, Japan). The IR images of temperature profile were obtained by a Fotric 225 Infrared Camera (Fotric Co., USA, error  $\leq 2\%$ ). To accurately measure the evaporation rates, the illuminated flocking board samples were floating on the water, and put on a properly calibrated electronic balance (Merrler Toledo ML503T, accuracy:  $1 \text{ mg}$ ). The evaporation weight change was measured every  $20 \text{ s}$ . The concentration of four primary ions was measured by an inductively coupled plasma optical emission spectrometry (PerkinElmer Instruments, USA).

## Supporting Information

Supporting Information is available from the Wiley Online Library or from the author.

## Acknowledgements

This work was jointly supported by the National Natural Science Foundation of China (grant nos. 11832010, 11890682, and 51706011), the National Key Basic Research Program of China (grant no. 2018YFA0208403), and the Science and Technology Program of Tianjin, China (grant no. 18YFYSZC00060).

## Conflict of Interest

The authors declare no conflict of interest.

## Keywords

3D designs, high evaporation rate, self-dissolution of salt, solar-driven evaporation, vertically aligned arrays

Received: April 25, 2019

Revised: July 9, 2019

Published online: August 5, 2019

- [1] L. Zhou, Y. Tan, J. Wang, W. Xu, Y. Yuan, W. Cai, S. Zhu, J. Zhu, *Nat. Photonics* **2016**, *10*, 393.
- [2] S. Surwade, S. Smirnov, I. Vlassioug, R. Unocic, G. Veith, S. Dai, S. Mahurin, *Nat. Nanotechnol.* **2015**, *10*, 459.
- [3] T. Ding, K. Liu, J. Li, G. Xue, Q. Chen, L. Huang, B. Hu, J. Zhou, *Adv. Funct. Mater.* **2017**, *27*, 1700551.
- [4] R. Sinha, *Modern Plant Physiology*, Alpha Science International, Pangbourne, UK **2004**.
- [5] M. Shatat, M. Worall, S. Riffat, *Sustainable Cities Soc.* **2013**, *9*, 67.
- [6] M. Mekonnen, A. Hoekstra, *Sci. Adv.* **2016**, *2*, e1500323.
- [7] D. Abbott, *Proc. IEEE* **2010**, *98*, 42.
- [8] I. Dincer, *Renewable Sustainable Energy Rev.* **2000**, *4*, 157.
- [9] H. Ghasemi, G. Ni, A. M. Marconnet, J. Loomis, S. Yerci, N. Miljkovic, G. Chen, *Nat. Commun.* **2014**, *5*, 4449.
- [10] Z. H. Wang, Y. M. Liu, P. Tao, Q. C. Shen, N. Yi, F. Y. Zhang, Q. L. Liu, C. Y. Song, D. Zhang, W. Shang, T. Deng, *Small* **2014**, *10*, 3234.
- [11] G. Tiwari, in *Solar Energy and Energy Conservation* (Eds: R. Kamal, K. P. Maheshwari, R. K. Sawhney), Wiley Eastern, New Delhi **1992**.
- [12] K. Soteris, *Energy* **1997**, *22*, 69.
- [13] L. Zhou, Y. Tan, D. Ji, B. Zhu, P. Zhang, J. Xu, Q. Gan, Z. Yu, J. Zhu, *Sci. Adv.* **2016**, *2*, e1501227.
- [14] G. Xue, K. Liu, Q. Chen, P. Yang, J. Li, T. Ding, J. Duan, B. Qi, J. Zhou, *ACS Appl. Mater. Interfaces* **2017**, *9*, 15052.
- [15] X. Wu, M. E. Robson, J. L. Phelps, J. S. Tan, B. Shao, G. Owens, H. L. Xu, *Nano Energy* **2019**, *56*, 708.
- [16] Y. Wang, L. Zhang, P. Wang, *ACS Sustainable Chem. Eng.* **2016**, *4*, 1223.
- [17] Z. C. Xiong, Y. J. Zhu, D. D. Qin, F. F. Chen, R. L. Yang, *Small* **2018**, *14*, 1803387.
- [18] P. P. Zhang, J. Li, L. X. Lv, Y. Zhao, L. Qu, *ACS Nano* **2017**, *11*, 5087.
- [19] H. Y. Ren, M. Tang, B. L. Guan, K. Wang, J. Yang, F. Wang, M. Wang, J. Shan, Z. Chen, D. Wei, H. L. Peng, Z. F. Liu, *Adv. Mater.* **2017**, *29*, 1702590.
- [20] Z. J. Liu, H. M. Song, D. X. Ji, C. Li, A. Cheney, Y. Liu, N. Zhang, X. Zeng, B. Chen, J. Gao, Y. Li, X. Liu, D. Aga, S. Jiang, Z. Yu, Q. Gan, *Global Challenges* **2017**, *1*, 1600003.
- [21] Q. M. Chen, Z. Q. Pei, Y. S. Xu, Z. Li, Y. Yang, Y. Wei, Y. Ji, *Chem. Sci.* **2018**, *9*, 623.
- [22] V. S. Mironov, M. Park, *Compos. Sci. Technol.* **2000**, *60*, 927.
- [23] A. Probst, R. Facius, R. Wirth, C. Moissl-Eichinger, *Appl. Environ. Microbiol.* **2010**, *76*, 5148.
- [24] H. Schmitz, *J. Therm. Biol.* **1994**, *19*, 403.
- [25] A. Lenert, E. Wang, *Sol. Energy* **2012**, *86*, 253.
- [26] X. Chen, J. N. Chen, X. L. Ouyang, Y. Song, R. Xu, P. X. Jiang, *Langmuir* **2017**, *33*, 6701.
- [27] M. Zhou, J. Yu, J. Li, B. Wu, W. Zhang, *Appl. Surf. Sci.* **2012**, *258*, 7596.
- [28] P. Mu, W. Bai, Z. Zhang, J. X. He, H. X. Sun, Z. Q. Zhu, W. D. Liang, A. Li, *J. Mater. Chem. A* **2018**, *6*, 18183.
- [29] Z. Zhang, P. Mu, J. X. He, Z. Q. Zhu, H. X. Sun, H. J. Wei, W. D. Liang, A. Li, *ChemSusChem* **2019**, *12*, 426.
- [30] P. Mu, Z. Zhang, W. Bai, J. X. He, H. X. Sun, Z. Q. Zhu, W. D. Liang, A. Li, *Adv. Energy Mater.* **2019**, *9*, 1802158.
- [31] X. Wu, L. M. Wu, J. Tan, G. Y. Chen, G. Owens, H. L. Xu, *J. Mater. Chem. A* **2018**, *6*, 12267.
- [32] W. Wagner, J. R. Cooper, A. Dittmann, J. Kijima, H. Kretzschmar, A. Kruse, R. Mares, K. Oguchi, H. Sato, I. Stocker, O. Sifner, Y. Takaishi, I. Tanishita, J. Trubenbach, Th. Willkommen, *J. Eng. Gas Turbines Power* **2000**, *122*, 150.
- [33] K. K. Liu, Q. S. Jiang, S. Tadepalli, R. Raliya, P. Biswas, R. Naik, S. Singamaneni, *ACS Appl. Mater. Interfaces* **2017**, *9*, 7675.
- [34] X. Q. Li, W. C. Xu, M. Y. Tang, L. Zhou, B. Zhu, S. Zhu, J. Zhu, *Proc. Natl. Acad. Sci. USA* **2016**, *113*, 13953.
- [35] H. M. Qiblawey, F. Banat, *Desalination* **2008**, *220*, 633.
- [36] M. W. Zhu, Y. J. Li, G. Chen, F. Jiang, Z. Yang, X. Luo, Y. Wang, S. Lacey, J. Dai, C. Wang, C. Jia, J. Wan, Y. Yao, A. Gong, B. Yang, Z. Yu, S. Das, L. Hu, *Adv. Mater.* **2017**, *29*, 1704107.
- [37] M. H. Sharqawy, V. J. H. Lienhard, S. M. Zubair, *Desalin. Water Treat.* **2010**, *16*, 354.
- [38] World Health Organization, *Guidelines for Drinking-Water Quality*, 4th ed., World Health Organization, Geneva, Switzerland **2011**.
- [39] F. Zhao, X. Y. Zhou, Y. Shi, X. Qian, M. Alexander, X. Zhao, S. Mendez, R. Yang, L. Qu, G. Yu, *Nat. Nanotechnol.* **2018**, *13*, 489.
- [40] X. Q. Li, J. L. Li, J. Y. Lu, N. Xu, C. Chen, X. Min, B. Zhu, H. Li, L. Zhou, S. Zhu, T. Zhang, J. Zhu, *Joule* **2018**, *2*, 1331.
- [41] H. M. Song, Y. H. Liu, Z. J. Liu, M. Singer, C. Li, A. Cheney, D. Ji, L. Zhou, N. Zhang, X. Zeng, Z. Bei, Z. Yu, S. Jiang, Q. Gan, *Adv. Sci.* **2018**, *5*, 1800222.